Aerospace Systems (2022) 5:47–63
https://doi.org/10.1007/s42401-021-00114-w

ORIGINAL PAPER

# Structural analysis of three-dimensional wings using finite element method

Abdul Aabid[1,2] · Muhammad Amir Mirza Bin Mohd Zakuan[2] · Sher Afghan Khan[2] · Yasser E. Ibrahim[1]

Received: 30 September 2020 / Revised: 6 October 2021 / Accepted: 14 October 2021 / Published online: 27 October 2021


## Abstract

This paper investigates the structural behaviour of the wing subjected to the aerodynamic loads during the flight using finite element analysis of wing flexure deformation. In this work, three different types of wing models are established. Material characteristics, the wing structure, and design principles have been taken into account. The assembly of the wing model consists of the thin skin, two spars, and the multi-ribs. The two spars consist of primary and secondary spars. For this study, NACA 23015 is chosen as the baseline airfoil as this airfoil is very similar to the customized airfoil being used in Airbus A320. Two spars mainly bear the bending moment and shear force, which are made of titanium alloy to ensure sufficient rigidity. The skin and wing ribs are made of aluminium alloy to lighten the structural weight; a static structural analysis is applied. Total deformation, equivalent elastic strain, and equivalent von Mises stress are obtained to study the wing's structural behaviour. Furthermore, the modal analysis is then applied. The natural frequencies and the modal shape of the wing for three orders are obtained through the pre-stress modal analysis. The modal analysis results help designers minimize excitation on the natural frequencies and prevent the wing from flutter. According to the results, designers can emphasize strengthening and testing the stress concentration and large deformation area.

**Keywords** Finite element method · Wing · Airfoil · Structural analysis · Simulation

## 1 Introduction

This research aims to quantify the structural behaviours of the three-dimensional wing as a wing structure. Its component plays a vital role in producing lift, provides stability, and offers excellent manoeuvrability to the aircraft. This article also proposes an analysis method for wing design models using the finite element method (FEM), including static structural and modal analysis. First, there will be three different types of wing models with different configurations consisting of a primary and secondary spar, thin skin, and multi-ribs. There will be a few limitations and assumptions made throughout the analysis. As a result, structural analysis of elastic strain, von Mises stress, bending, and torsional moment of the wing obtained through transient structural analysis, which applies for optimization and improvement to the design of the wing for the future. The same step of analysis is repeated to analyse the other two different wing models. A fatal accident can happen to the wing structure due to complicated external flight environments, which will result in the pressure of upper and lower wing surfaces with varying aerodynamic flow fields around the wing [23]. The modal analysis investigates the resonance frequencies of the wing computationally as structure oscillations at resonance frequencies are often hazardous since relatively small excitation forces can develop large-amplitude vibrations, leading to structural failure.

The studies have been found on structural analysis using the mathematical expressions; for example, in 1943, Flax [6] derived the number of equations for wing-aileron. Next, the numerical model was designed and simulated the structural analysis results for a three-dimensional swept wing [14]. A three-dimensional wing scan of a dragonfly fore- and hind-wing with a micro-CT scanner has been performed for the analysis [9]. Garmann et al. [7] conducted a numerical study on the three-dimensional wing and resolved the flow of struc-

✉ Abdul Aabid
aaabid@psu.edu.sa; aabidhussain.ae@gmail.com

1 Department of Engineering Management, College of Engineering, Prince Sultan University, PO BOX 66833, Riyadh 11586, Saudi Arabia

2 Department of Mechanical Engineering, Faculty of Engineering, International Islamic University, Malaysia, 53100 Kuala Lumpur, Malaysia

ture and aerodynamic loading. A comparative study on the three-dimensional wing for aerodynamics drag with design and analysis propose was drawn by the authors [5]. Like the present study, static and dynamic loading conditions on the spacecraft structural component were adopted to analyse the load superposition [19]. Also, numerical investigation of the transonic buffet on a three-dimensional wing using incremental mode decomposition by the authors [16]. Yang et al. [21] numerically investigated the thickness of aircraft wing skins with optimization studies using the ABAQUS commercial tool. Lorber [13] studied the compressibility effects on a three-dimensional wing dynamics stall. Garre [8] investigated the bending and shear loads on a wing by modelling the components—ribs and spars—and their effects considering the structural analysis. In some studies, wing weight has also been majored by varying the spacing between the ribs and stringer and its effect on weight considering aluminium material [3]. Kumar et al. [12] designed an aircraft wing structure for static analysis and fatigue life prediction using FE analysis via ANSYS APDL and determined the fatigue to predict the life of wing structures. The obtained results from 3D modelling in ANSYS shows an optimum result that can be further used to evaluate the damage tolerance for the complete evaluation of damage tolerance.

Structural analysis of an aircraft is vital to keep flying safely. The plane's study includes designing any aircraft components to resist stress from any deformation that occurs. Zakuan et al. [22] investigated the three-dimensional wing's structural behaviour imperiled to flowing loads. For the wing model establishment and the maximum operating Mach number of Airbus A320 is equivalent to 0.82, which is slightly lower operating speeds than its predecessor, A300 and A310. Usually, the aircraft's cruise speed must range from Mach number 0.79 to 0.80 [15]. On the other side, few studies from Zhang et al. [23] and Vani et al. [18] describe a wing model's development based on their own goals. This can be seen when Zhang et al. [23] set up a wing based on a large aspect ratio design. It is more effective to evaluate a considerable aspect ratio wing design to study wing deformation. Vani et al. [18] modelled an A320 wing prototype with a scaled-down model. At the initial design stage, testing a full-scale model is avoided. Because of the size of the wing to be reproduced and assembled, a scaled-down model is selected. But in this paper, the wing structure is set to be 1:1. According to Raymer [17], the reference wing is the primary wing geometry used to begin the layout. For a three-dimensional wing, the air can escape around the wingtip. The pressure difference between upper and lower surfaces will drop due to air fleeing, thus reducing the lift near the tip.

In recent years, a 3D wing was designed for different vehicles such as hovering flight [20], airborne wind energy generation [4], and unmanned aerial vehicles [10]. In addition, the wing has been designed with a tapered ratio [1] to investigate the normal mode analysis and the linear static structure for transport aircraft application purposes. In these previous studies, the FEM was used and successfully determined the structural analysis and optimization for a specific design and application. They are conducted the linear/non-linear, static/dynamics, and structural/mode analysis to determine the stresses, strains, deformation, and safety factor of the wing at different loading conditions and material properties. After literature studies, it has been clear that the swept wing is used in modern aircraft industries to which wing sweep is applied primarily to reduce the drag divergence Mach number. Besides, in-plane wing's structure, the ribs will give shape to the wing, and the spar will account for most of the bending loads on the wing structure. In a fixed-wing plane, the spar is the wing's primary structural member, running spanwise at the right angles to the fuselage. Hence, this study focused on the wing structures using different types to extract the structural performance with the finite element analysis (FEA).

## 2 Finite element method

The structural analysis of any component such as aircraft parts using computational tools is easier to predict the results [16]. In this work, an aircraft primary structural component 3D wing has been analysed by considering three different aspects/designs to predict and compare the simulation results, which will be helpful to further investigate with experimental work and practical applications. The materials used to design the wing with mechanical properties have been illustrated in this section. The methodology to design and build a three-dimensional wing with SolidWorks is a robust computer-aided design (CAD) and computer-aided engineering (CAE) program. Moreover, to analyse the designed model, an ANSYS static structural analysis through the workbench is used to evaluate and examine the model wing's behaviours. Generally, this has been considered through the FEM, which only provides an approximate solution to the problem. Besides, it is used as the basis for modern simulation software and helps engineers to find weak spots, maximum and minimum von Mises stress, total deformation in their designs.

### 2.1 Structural and static analysis

In this section, the structural and static analyses will be elucidated and explained before starting the wing design and analysis. As mentioned earlier, a statistical approach is used in this work. The literature shows that different types of wings have been utilized for numerical examples, and some have rarely been used. In the current study, an Airbus A320 with a single-aisle configuration is chosen for the sample (Table 1).

**Table 1** General specifications for Airbus A320

| Parameter | | |
|---|---|---|
| Wingspan | | 33.910 m |
| Semi-span | | 16.95501 m |
| Aircraft maximum weight | MTOW | 68,000 kg |
| | MLW | 63,000 kg |
| | MZFW | 59,000 kg |
| | MW | 39,000 kg |
| Maximum passenger | | 180 people |
| Operating limit speed | MMO | 0.82 |
| | Cruise speed | 0.79–0.80 |
| Airfoil | Root airfoil | NACA 23015 |
| | Kink airfoil | NACA 5-digit |
| | Tip airfoil | NACA 5-digit |
| | Root chord length | 7.05/3.525 m |
| | Tip chord length | 1.50/3.525 m |
| Skin thickness | | 9.1 mm |
| | Position of front spars | 20% of the chord m |
| | Position of rear spars | 65% of the chord m |

Since there are many limitations and the wing structure complexity, it is incredibly time-consuming, if not impossible, to carry out.

The model's geometry is simplified by decreasing the wing scale and omitting numbers of ribs as they do not contribute against bending. For static analysis, a factor of safety is considered to acquire the pressure on the surface of the wing and the lift load. The actual load-bearing capacity of a structure or component and the required margin of safety for a structure is decided based on the code, law, and design requirements. An FoS on the loading factor accounts for extreme loading due to human error or unexpected weather conditions such as gust load. Therefore, the FoS is selected to be 1.5, and thus the produced lift for the wing is calculated.

First, the aircraft's weight is determined by multiplying the maximum take-off mass of the aircraft with the gravitational acceleration. It is essential to note that the aircraft's maximum take-off weight should be taken as the initial mass.

$$\text{Weight, W(N)} = 68,000\text{kg} \times 9.81\frac{\text{m}}{\text{s}^2} = 667,080\text{N}, \quad (1)$$

$$\eta_{\max} \times \text{FoS} = \frac{\text{L}}{0.4(\text{W})}, \quad (2)$$

$$\begin{aligned} L_{\text{total}} &= (\eta_{\max} \times \text{FoS}) \times 0.4\,(\text{W}) \\ &= (3.5 \times 1.5) \times 0.4\,(667,080) = 1,400,868\text{N}. \end{aligned} \quad (3)$$

After the total lift load acting on the wing is calculated, the lift load is then divided into two, as the aircraft is symmetric.

**Table 2** Design of wings and spars and their characteristics

| No. | Design | Characteristics |
|---|---|---|
| 1 | Design 1 | The straight wing comprises two spars with a solid square cross section, which is a primary and secondary spar. The wing also has ten ribs |
| 2 | Design 2 | The straight-wing comprises two spars that have an I-shaped cross section, which is a primary and secondary spar. The wing also has ten ribs |
| 3 | Design 3 | Tapered wing |

Initially, there is only 80% of the lift load is applied on the wings, and the remaining 20% is applied on the fuselage. The lifting load is considered an important criterion while designing an aircraft. Therefore, only 80% of the total lift load is considered on the wing.

$$L_{\text{wing}} = 0.8\,(L_{\text{total}}) = 0.8 \times 1,400,868\text{N} = 1,120,694.4\text{N}, \quad (4)$$

$$L_{\text{eachwing}} = \frac{1,120,694.40\text{N}}{2} = 560,347.20\text{N}, \quad (5)$$

$$\begin{aligned} \text{Pressure, } P\,(\text{Pa}) &= \frac{\text{Lift, } L}{\text{Wingarea, } S} = \frac{560,347.20\text{N}}{122.5\text{m}^2} \\ &= 4574.263\text{Pa}. \end{aligned} \quad (6)$$

Therefore, the pressure due to the lift load on the lower surface of the wing is 4574.263 Pa.

## 2.2 Geometry and modelling

A designed wing modelled exported into the Para solid file that ANSYS Workbench can read for the analysis. Three designs of the wing model and two different types of the cross section of the spar are established to analyse and understand the wing's structural behaviour—all design of wings that is characterized as follows (Table 2). The three designs of wings are because of the limitation and boundaries present in designing the Airbus A320 wing. As stated in the previous section, aircraft manufacturers' secrecy made it impossible to gather and obtain information directly from these organizations, especially the industry's leading players, Boeing, and Airbus. All three wing designs of aircraft are explained and elucidated in detail. The steps and boundaries are considered to obtain and achieve an accurate result for structural behaviour analysis.

There are about five steps to design and analyse the wing. The coordinate of the point of NACA 23015 airfoil is obtained to build a wing. In the airfoil generator, the design coefficient of lift of 0.3 is chosen and the points coordinate is saved in a text file. The coordinate file of NACA 23015 is chosen to be exported into the SolidWorks and the base plane

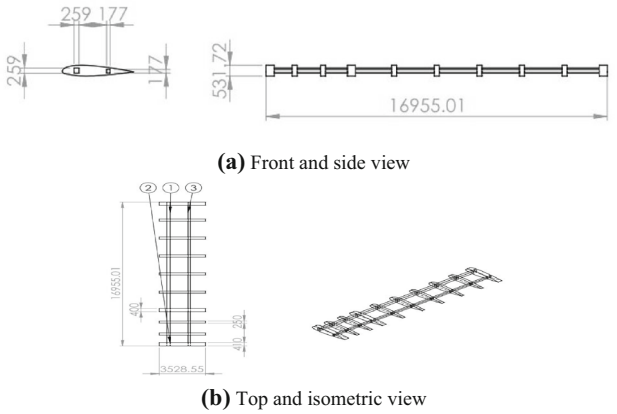


**(a)** Front and side view

**(b)** Top and isometric view

**Fig. 1** Straight wing comprises of square cross-sectional spars/rib

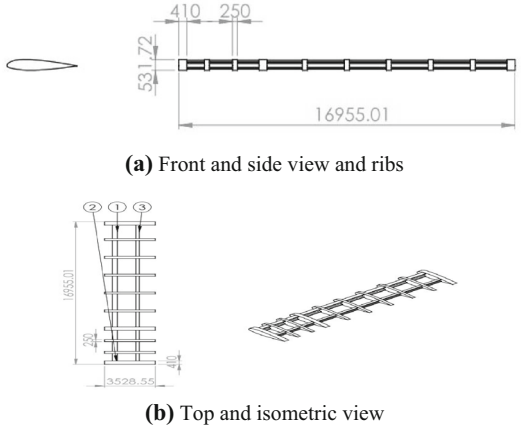


**(a)** Front and side view and ribs

**(b)** Top and isometric view

**Fig. 2** Straight-wing comprises of I-shaped cross-sectional spars

for the point coordinates is set up to be plotted in *XY*-plane. The airfoil tool generator generates the point coordinates in the *x*-, *y*-, and *z*-axes. The point coordinates are then converted into an excel sheet file for SolidWorks to read the coordinates accordingly. An airfoil has been built at a different location on the coordinate system to model the wing, the first airfoil is plotted on the front plane; another curve line of an airfoil is planned on one reference plane Plane1. Additionally, the same step is chosen to plot other NACA 23015 airfoil ribs. Then the design of the wing is continued with the addition of 9.1 mm thin skin layer. It is important to note that all wings design used the same airfoil family with a wingspan of 16,955.01 mm. After completing, the wing layout can be analysed and simulated in the ANSYS Workbench using both static structural and modal analyses.

Design 1—straight wing with square spars: the first design of the wing model is a straight wing comprised of square cross-sectional spars and ten numbers of ribs as shown in Fig. 1.

Design 2—straight wing with I-shaped spar: for the second design of the straight wing, the steps taken into consideration are similar to what has been done in the wing model's first design. Figure 2 shows the details of wing structures.

Design 3—tapered wing: for the tapered wing, the same steps are considered in designing and modelling the wing model. Through a finite element model, the dimensions of the tapered wing are shown in Fig. 3.

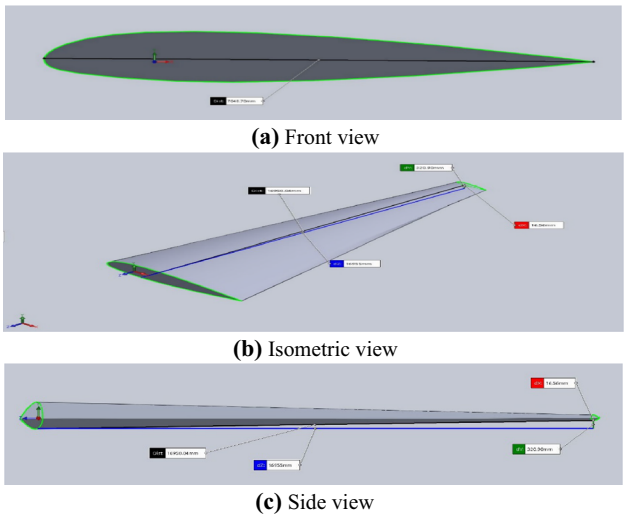

**(a)** Front view

**(b)** Isometric view

**(c)** Side view

**Fig. 3** Tapered wing together with its measurement

## 2.3 Meshing and boundary conditions

For the meshing of the finite element model for structural analysis, the number of elements and nodes should be acceptable for the relevant result. Some definitions need to be set up first before generating the mesh. Mesh defeaturing, capture curvature, and capture proximity in the sizing section are included to obtain a better mesh result. For the mesh analysis, a magnificent mesh is needed to obtain accuracy in results. The element sizing for both closed and open cross sections is set to be 0.1 m with a coarse relevance centre and medium transition for the present investigation's inflation option. Therefore, as an illustration, both solid square and I-shaped beam mesh analyses are shown in Fig. 4. A minimum length of the edge is critical to meet the requirement to mesh each part's model. But present models focus more on the structural type of mesh, and near to the high strength region, a very fine mesh was used with a higher number of elements/nodes to track the optimum results. The shape is considered rectangular in each section of the wing.

After defining the edge size of 0.1 m during the mesh creation of each cross section for all designs, the minimum edge length was obtained through the ANSYS mesh tool. It was found that design 1 of 0.1770 m, design 2 of 5.27e−002 m, and design 3 of 9.8425e−005 m for open and closed cross-sections is limited to the ANSYS recommendation for the

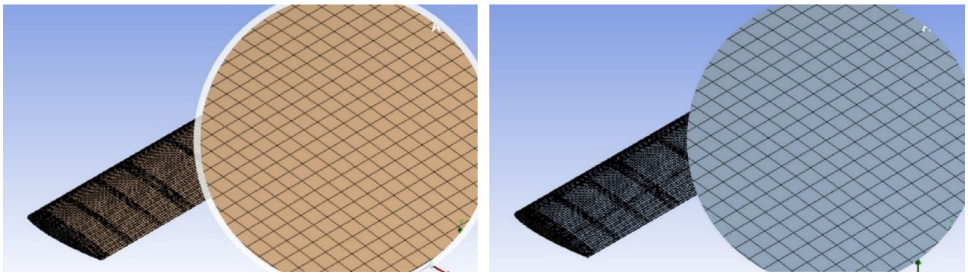

**(a)** square spars **(b)** I-Shaped spars

**Fig. 4** Mesh preview together with the close-up view for the straight wing

mesh size based on the model. Moreover, in the present case, the elements (nodes) of each model have 35814 (82962), 141254 (682161), and 10076 (10272) for design 1, design 2, and design 3, respectively. However, the mesh model indicated all the inputs defined are suitable for the structural analysis [2]. Since designs 1 and 2 have a different subsection. For the square and I-shaped part to control the mesh size, the object multizone quadrilateral/tri-method was fully defined with a minimum edge of 7.2623 m for each design with free face all quadrilateral mesh type with the mesh size 1.

It is seen from Fig. 5a, b that the face meshing on the skin surface of the wing is a structured mesh. Face meshing, body sizing, and multizone meshing have been applied for the first two wing designs, and the result of meshing turns out the structured one, which is more accurate than the unstructured one. On the other hand, it can be seen that the face meshing on the tapered wing is partially unstructured. Some changes have been made to correct and debugging the face meshing, but the results have remained constant. This may be due to the uneven surfaces of the wing skin loft. As for the wing's skin, which is on the top and bottom surfaces, the result of the face meshing is structured. Thus, the static and modal analysis obtained later will have accurate and better results compared to the unstructured face meshing.

After designing and modelling the spar beam, boundary conditions needed to be applied to analyse static structural and modal analysis. Both spar beams are used with a pressure load force at a *y*-component of 4000 Pa on the bottom surface and fixed support at one end of the beam. Figure 6 illustrates the wing's boundary conditions. The location of improved support at the root chord of the wing structure is shown in blue arrow signs, Fig. 6a. In contrast, a uniform pressure lift load is applied at the wing structure's bottom surface, indicating the red arrow sign Fig. 6b.

As illustrated in Fig. 6, two analysis settings and boundaries are set to analyse the wing's static structural and modal analysis. Two boundaries that are applied are fixed support and a vertical pressure load at the *y*-component. The fixed support is used at one end of the wing because it is attached to the aircraft's fuselage. Therefore, one end that is bigger in terms of the surface area is selected as there will be more load. For instance, landing gear and engine nacelles are located at the wing's inner side since the area at that position is much spacious compared to the location at the wingtip. About 4000 Pa of pressure lift load is applied on the *y*-component of the surface of the wing. Since the result is trivial due to the complexity of the shape is low. Therefore, the mesh should appear to be a structured one. One of the significant benefits is that the nodal neighbour connectivity is simple and easy compared to the unstructured one. The simplicity of nodal neighbour connectivity will simplify the program. Hence, the accuracy of the result for the geometry will increase if it is a structured mesh.

## 3 Material selection

In material selection, many aspects and factors need to be considered as several properties are essential to the choice of materials for an aircraft. The range of the best material depends upon the application. As mentioned earlier, many factors need to be considered before selecting the material. Therefore, due to the factors listed above, titanium is chosen as the wing spar material. Since the wing spars are the primary members of the wing structure, a material with a higher yield and ultimate strength, high fracture toughness, high stiffness, and high resistance to the fatigue crack is selected. Additionally, higher resistance to creep, higher corrosion resistance, and higher temperature limits are needed to take into consideration. Thus, for these reasons, titanium seems to be the ideal spars material. It has a better strength-to-weight ratio and stiffness than aluminium and is capable of temperatures almost high as steel [17].

In the selection of the material of the wing, two types of material are chosen. The materials are aluminium alloy and titanium alloy. Aluminium alloy is selected as the skin's material to reduce the weight of the wing structure. The aluminium alloy has a higher resistance to corrosion and lower weight compared to steel alloys. The aluminium is used for parts like the wings, where low mass and elasticity are more critical. Meanwhile, ribs and wing skin materials have aluminium alloy, whereas primary and secondary components

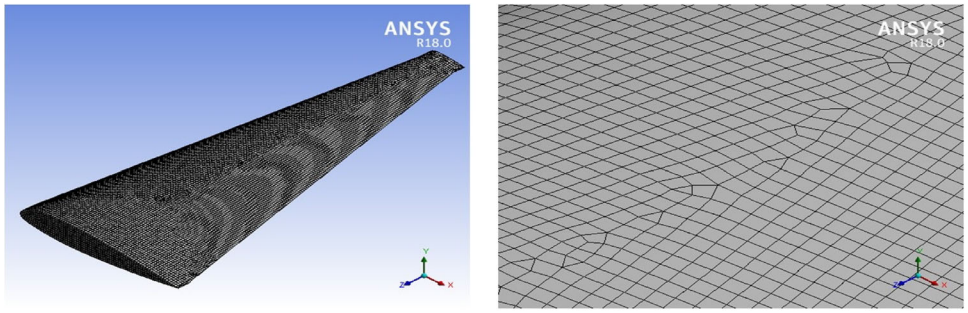


**Fig. 5** Mesh preview together with the close-up view for the tapered wing

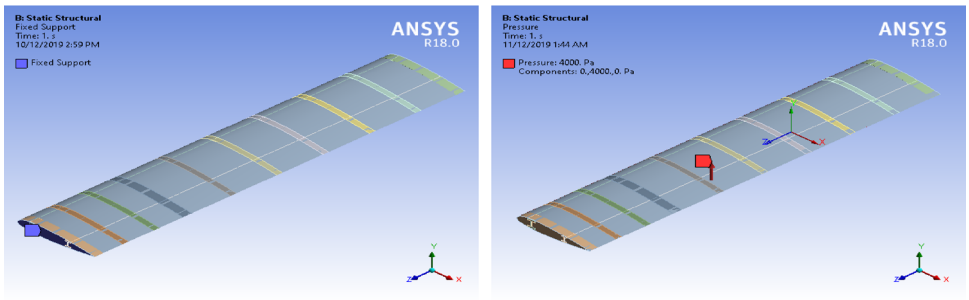


**Fig. 6** Applied boundary conditions

**(a)** Fixed support **(b)** Pressure

**Table 3** Mechanical properties of titanium and aluminium alloy

| Materials | Titanium alloy | Aluminium alloy |
|---|---|---|
| Poisson ratio | 0.36 | 0.33 |
| Young's modulus | $9.6 \times 10^{10}$ Pa | $7.1 \times 10^{10}$ Pa |
| Compressive yield strength | $9.3 \times 10^{8}$ Pa | $2.8 \times 10^{8}$ Pa |
| Tensile yield strength | $9.3 \times 10^{8}$ Pa | $2.8 \times 10^{8}$ Pa |
| Shear modulus | $3.2594 \times 10^{10}$ Pa | $2.6692 \times 10^{10}$ Pa |

have titanium alloy. Table 3 shows the properties of materials of the selected materials.

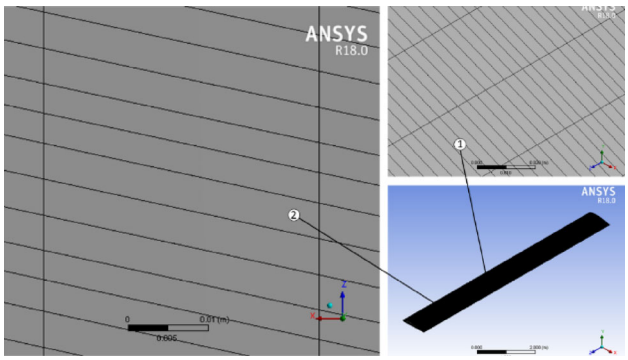


**Fig. 7** Close-up view of the mesh

## 4 Results and discussion

As a result, a validation/comparison is established to be on par and improve the quality of this research and processes by comparing results. It is not easy to obtain the experimental results for such cases. Wind tunnel test results were found but not precisely in the present case. Konayapalli and Sujatha's [11] work is similar to the present study and was chosen for the comparison of results and validation. This research paper deals with designing and analysing a general aviation aeroplane using a NACA 4412 wing airfoil. Indeed, this has not consideration exactly as validation of results since it does not include any experimentation, but the results chose to compare our products to justify the present work. In the past, the researchers used CATIA V5 and ANSYS 14.5 to examine the wing's reliability. The steps that are mentioned before are taken into considerations to validate the results. An aluminium alloy of material is applied to the wing structure, and the aircraft wing has meshed (Fig. 7). The boundary condition is set up for the finite element analysis, and one end of the wing, which is the root, is supported with fixed support. Then the pressure is applied to the wing, and the analysis is done. The result of the validation is shown in Fig. 8.

A complete deformation has been obtained for comparison of performance, which is useful for wing analysis. As the wing is subjected to load values, the overall deformation of the wing is obtained, and the components of the wing structure proposal are suggested; each component must have progressive deformation gradually as it moves away from the supports. As can be seen in Fig. 8, the maximal deformation of the wing occurs as predicted at the wingtip with a value of 61.02 cm; this value can be considered suitable for a

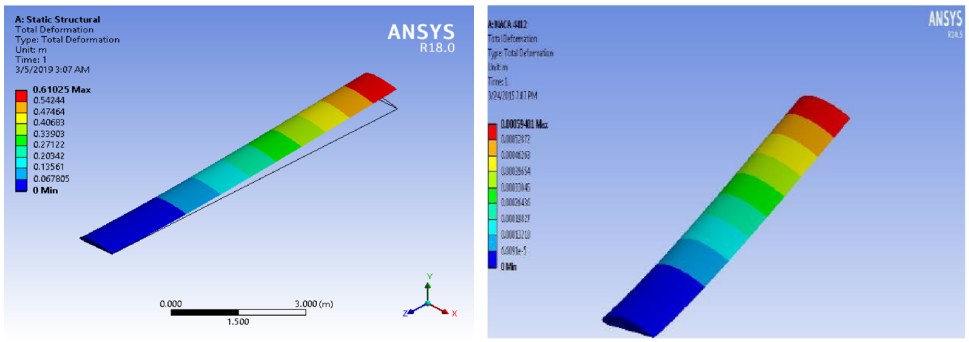


(a) (b)

**Fig. 8** Total deformation for the wing structure with NACA 4412 airfoil. **a** Current work; **b** previous work [11]

wing of 4.5 m, particularly when considering that the normal deformation of a glider's wings is high in comparison to its size.

From the ANSYS simulation and analysis, the results obtained are not precisely the same as the material selection used in the past paper is an aluminium alloy of AA7075. Since the engineering material library for ANSYS does not provide a complete mechanical property of AA7075 type of aluminium alloy, changes have been made with the consideration of aluminium alloy. The density is considerably high since aluminium alloy density is about 2700 kg/m$^3$ while 2810 kg/m$^3$ is for AA7075. That is approximately a 3.91% percentage error in terms of material's density. This will result in the total deformation result of the wing analysis. For comparison, the overall deformation from the previous study is 0.59481 m.

In contrast, the current simulation total deformation is 0.61025 m, which is an acceptable difference between the prior research, and the percentage difference is 2.53%. This difference could be due to the different numbers of elements and nodes used and primarily due to the material selection, even though it is in the same alloy family. It is also observed that material selection is vital to analyse a structure since every material has its tensile strength, ultimate load strength. On the other hand, the difference also may be due to the different number of elements and nodes used for meshing analysis. Hence, this validation/comparison can be successful since the total deformation results are approximately similar to the previous study. It is essential to remember that the steps taken into consideration to complete the analysis can be correct since the review process is identical.

## 4.1 Data analysis and interpretation

Due to the design's nature that would make FEA imprecise and too time-intensive, the template's geometry is simplified by omitting the stringers if not impractical. The model is produced using the given dimensions and pressure load and applying a fixed constraint to the wing root, and FEA is performed.

### 4.1.1 Static structural analysis

Static structural modelling is used to evaluate the wing as it is not associated with time movement. The purpose of this analysis is to examine the mechanical nature of a three-dimensional wing with no change in time. Static structural analysis is, therefore, the best choice for analysing the functional actions of the wing.

**Design 1: straight wing with square spars** The first wing model design, which is a straight wing configured with two solid square spars and ribs, experienced a total deflection of 1.6339 m at the tip of the wing. This caused zero deformation there when a pressure load is applied. Both views can be seen in Fig. 9a, zero deflection happened at the root, and the distortion started to increase along the wing's span.

When the wing is subjected to the load values, the overall deformation of the wing is obtained, and the components of the wing structure proposed, each component must have progressive deformation gradually as it changes away from the supports. As seen in Figs. 9a, 10a, and 11a, the maximal deformation of the wing occurs as predicted at the wingtip with a value of 163.39 cm, 15.866 cm, and 23.904 cm; this value can be considered suitable for a wing of 8.48 m, particularly when considering that the normal deformation of a glider's wings is high in comparison to its height. Still, it reduced when the secondary structural component (design 2) reduces, and a tapered ratio (design 3) was found. The stress data should be compared to the safety factor, and the safety factor will be achieved if the dimensioning of the parts that make up the plane is checked or, on the other hand, if there are no good idea design support charges imposed from a geometrical and material standpoint. The equivalent value of the maximal stress is seen in Fig. 9b. More stressed areas are close to the supports and benefits equal to or greater than this

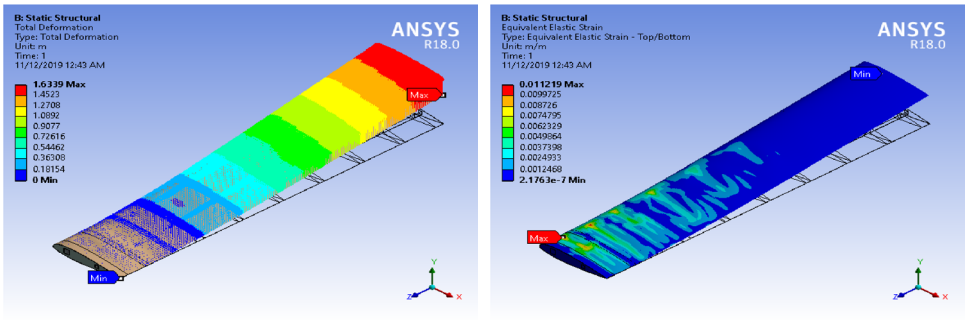


**(a)** Total deformation **(b)** Equivalent elastic strain

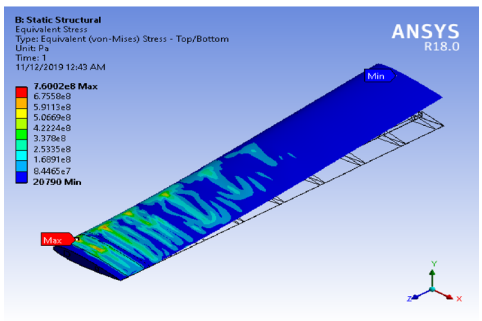


**(b)** Equivalent (Von-Mises) stress

**Fig. 9** Straight wing configured with square spars and ribs

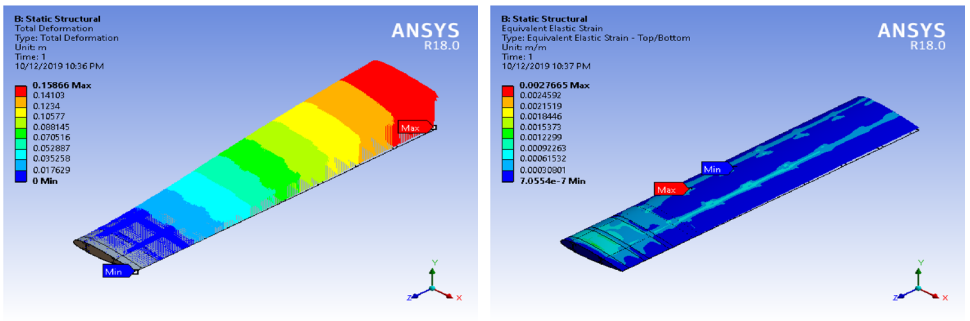


**(a)** Total deformation **(b)** Equivalent elastic strain

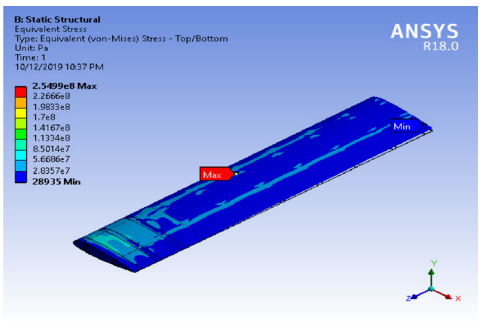


**(c)** Equivalent (Von-Mises) stress

**Fig. 10** The straight-wing configured with I-shaped spars

effort to the wing's first–second rib. The element that helps the whole plane bending it has the highest importance.

When a material's von Mises stress exceeds a critical value known as the yield strength, it is said to start yielding. The von Mises stress is used to predict material yielding under any loading environment from the effects of basic uniaxial tensile checks. The property that two stress conditions with equal distortion energy have equal von Mises stress is satisfied by the von Mises stress. A physical explanation of von Mises's criteria, claiming that yields occur as the elastic energy of distortion exceeds a critical point. The maximal distortion strain energy criterion is another name for the von Mises cri-

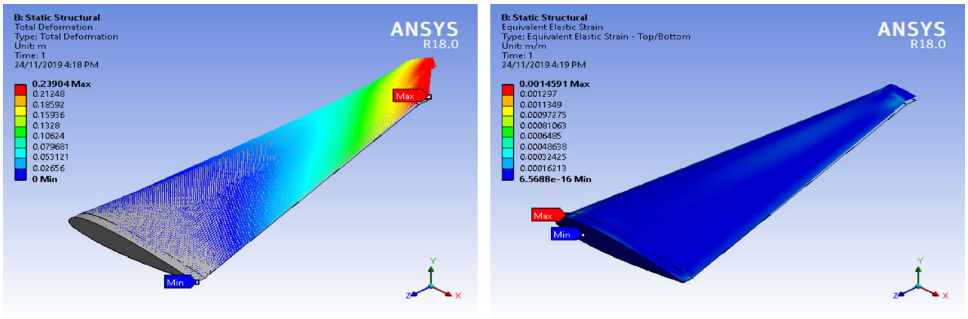


**(a)** Total deformation **(b)** Equivalent elastic strain

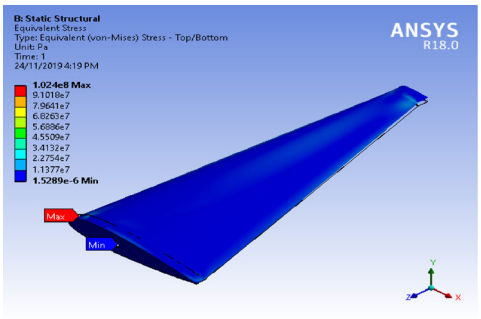


**(c)** Equivalent (Von-Mises) stress

**Fig. 11** The tapered wing configured without any internal ribs and spars

terion. In the present investigation, the maximum von Mises stress was found for design one $7.6002 \times 10^8$ Pa, whereas design two follows with $2.5499 \times 10^8$ pa and design three $1.0248 \times 10^8$ Pa. It indicates that high strength will depend on the secondary structural component and cross-sectional area ratio of the wing (tapered).

The maximum equivalent elastic strain and equivalent (von Mises) stress happened between the first and second ribs at the inboard of the wing structure. At the root of the wing design, fixed support is applied, and there is a presence of a reaction force that will counter and resist the pressure load. As shown in Fig. 9b, c, there are three reaction forces present in the fixed support reactions: horizontal and vertical forces and the moment at point A at the fixed support reaction.

**Design 2: straight wing with I beam spars** In the other wing model design, a straight wing configured with two I-shaped cross-sectional spars and ribs, the maximum total deflection is about 0.15866 m. The wing structure's deflection started on the second spars in the inboard section of the wing, with a 0.017629 m of displacement in the vertical direction. The deflection is a pure bending mode in the vertical direction (Fig. 10a).

The maximum value of equivalent elastic strain and equivalent (von Mises) stress is located at the fifth and sixth ribs from the wing structure's root. This is due to the I-shaped beam spar effect that prevents the equivalent elastic strain from increasing at the root of the wing structure. Figure 10b, c shows that the lowest equivalent elastic strain and equivalent (von Mises) stress developed are at the root. This is due to the fixed support's reaction forces to resist and counter the pressure load acting on the wing's bottom surface. The minimum value of strain and stress developed at the root around the centre, the maximum amount of strain and stress are turned up.

**Design 3: tapered wing** Figure 11a shows that the maximum overall deflection of tapered wing configured without any internal ribs and spar's structure developed at the wingtip of the wing. The gross distortion built upon this wing structure is a combination of bending and twisting modes. Notably, the total deformation is building up at the trailing edge of the wingtip. This is a precise observation that bending, and the twisting mode of deformation are developed at that location. This has resulted in a 0.23904 m of deflection at the trailing edge of the wingtip alone since the highest total deformation is located. The zero deflection happened at the root of the wing.

The equivalent elastic strain and equivalent (von Mises) stress, the maximum values of both strain and stress developed at the first rib from the wing structure's root. The development of maximum elastic strain and equivalent (von Mises) stress located on the root of the wing, there is fixed support situated at one end of the wing, which is the root of the wing structure. Hence, three reaction forces correspond to the selection of fixed support as a support on the aircraft (Fig. 11b, c).

**Table 4** Comparison of results

| Wing design model | Total deflection | Equivalent elastic strain | Equivalent (von Mises) stress |
|---|---|---|---|
| Straight wing configured with square cross-section spars and ribs | 1.6339 m | 0.011219 | $7.6002 \times 10^8$ Pa |
| Straight wing configured with I-shaped cross-section spars and ribs | 0.15866 m | 0.0027665 | $2.5499 \times 10^8$ Pa |
| Tapered wing configured without any internal ribs and spars | 0.23904 m | 0.0014591 | $1.024 \times 10^8$ Pa |

**Comparisons** Table 4 illustrates the comparison of results for static structural analysis of the wing design model's three different configurations. It is seen that the maximum total deflection for a straight wing configured with square cross-section spars and ribs is larger than the other two wings design model—a straight wing set with I-shaped cross-section with spars and ribs. Also, the tapered wing is configured with no internal ribs and spars. The value for the total deflection of the straight wing with square spars is 1.6339 m, which is about 164.6% greater than the straight-wing configured with I-shaped cross-sectional spars, the lowest total deflection. Although a wing structure design is equipped with primary and secondary spars and ribs, where the spars tend to counter the shear and bending forces developed due to the external pressure load, the effect of cross-sectional shape is still essential. For 164.6% of increment in the wing's deformation, the structure will lead to a significant fatality and disaster to aviation and aerospace industries. The selection of suitable cross-sectional area and shape of spars are essential to design a wing structure model.

The total deflection for the tapered wing without any internal spars and ribs is the second highest, with a value of 0.23904 m. That is about 40.43% of increment compared to the straight wing configured with the I-shaped cross-sectional spars. Besides the equivalent elastic strain and equivalent (von Mises) stress, again, the straight wing configured with solid square spars and ribs built up the highest value of strain and stress compared to the straight wing with I-shaped spars and ribs as well as the tapered wing. The total deflection for the straight wing with square spars and ribs is 0.011219 m/m, which is about 153.9% higher than the tapered wing since the tapered wing develops the lowest equivalent elastic strain as the von Mises stress. The taper ratio of the wing structure is affecting the value of elastic strain and von Mises stress significantly.

Similarly, the equivalent von Mises stress of the straight wing with square spars and ribs is the highest among all three. The value is $7.6002 \times 10^8$ Pa, which is 152.5% higher than the tapered wing's lowest one. From this observation, it may be concluded that a tapered wing structure is the best choice due to its higher efficiency in the structure and aerodynamics. As for the straight wing configured with I-shaped spars and ribs, the choice of I-shaped cross-section is the best compared to solid square spars because of its capability to resist shear and bending more efficiently than the square cross-section. For the most part, a wing with a taper ratio is more desirable to be selected. When a rectangular wing is tapered, the tip chords become shorter, eliminating the undesired effects of the rectangular wing with the constant chord. Therefore, a tapered wing is the preferable one to be selected as a wing model design.

## 4.2 Modal analysis

Modal analysis is a process to determine the vibration characteristics (natural frequencies and mode shapes) of a structure or a machine component. Therefore, all three design models of wing structure are to be analysed to obtain the resonance frequency and respective modal shape.

### 4.2.1 Design 1: straight wing with square spars

The first mode of vibration for the wing model's first design is pure bending mode in a vertical direction with a natural frequency of 0.64301 Hz. The wing structure appears to bend upward in a vertical direction. That is because the wing is tending to bend about the root section's minimum moment of inertia. Apart from this, there is no support at the wing's tip chords to resist and overcome the applied load in the *y*-direction, located at the bottom of the wing. It is seen in Fig. 12a that the maximum total deformation is developed at the tip chords of the wing with 0.012837 m, while zero distortion happened at the root. In the second mode of vibration, a pure bending mode in a vertical direction with a natural frequency of 4.195 Hz is observed. The wing appears to bend upward at the centre of the wing structure, and at the top chords of the wing, it bends downward. It is seen from Fig. 12b that the maximum deformation is at the centre of the wing structure, with 0.019954 m of deflection. The primary solid square spar mainly causes deflection at the centre of the wing structure. The spar has started to deform and bend, where the deflection is seen at the second ribs from the root chord of the wing. Consequently, another bending at the tip chord of the wing has started to develop. Therefore, the only

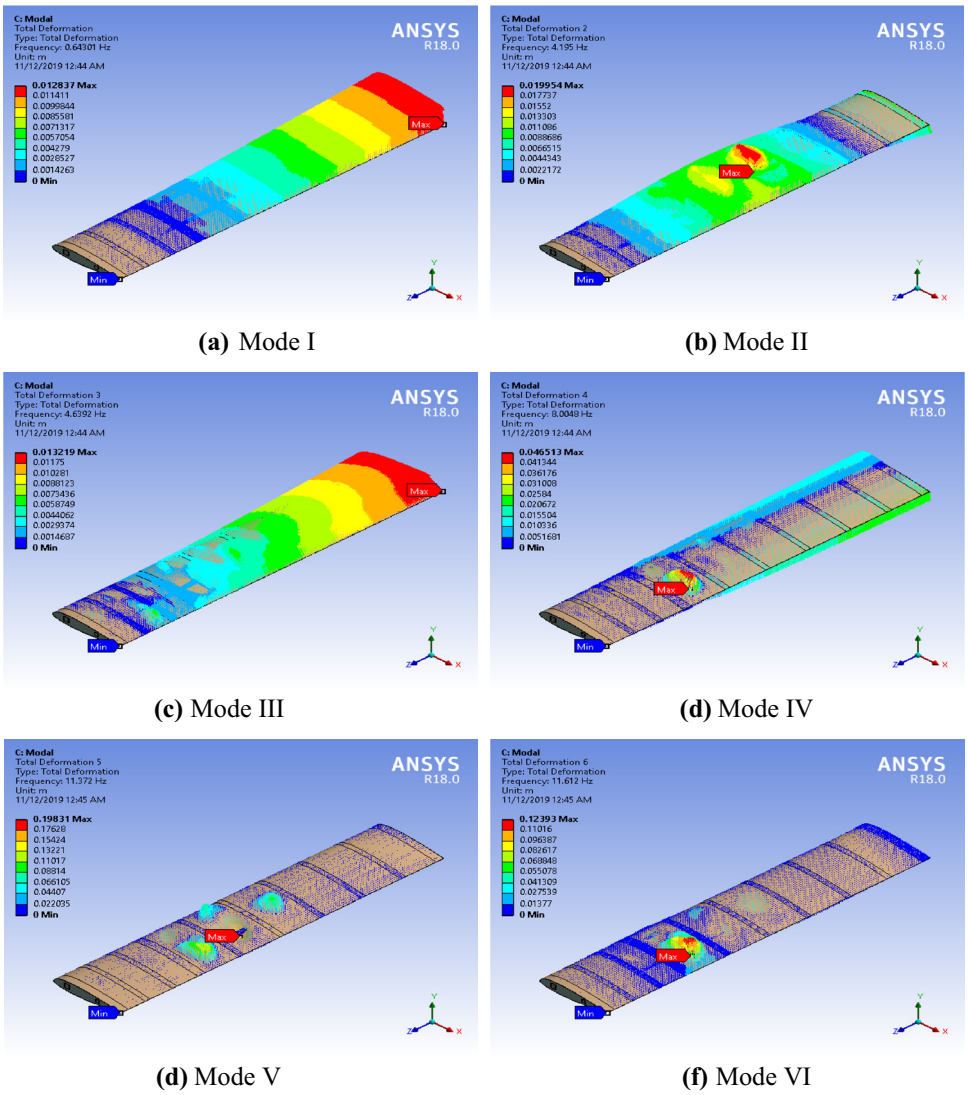


**Fig. 12** Model analysis of straight wing configured with square spars and ribs

reason why this happens is that the solid square spar cannot resist the applied pressure load at the bottom surface of the wing. In the analysis of wing spar before, the square cross-section spar has less moment of inertia than the I-shaped cross-section spar, which could be one reason why higher deflection developed at the solid square cross-section spar.

The third mode of vibrations for straight wing configured with two square cross-section spars and ribs, a bending and twisting mode, is built when a natural frequency is 4.6392 Hz. The wing model experienced a bending failure in the horizontal direction and a twist in a clockwise direction. It is observed from the front view of Fig. 12c that a twist from the bottom surface of the wing to the top happened at the trailing edge of the tip chord of the wing. The maximum total deflection is built at the wing's trailing edge with 0.013219 m of deformation, whereas zero distortion is happening at the root chord of the wing. As mentioned earlier in two or three analyses before, it is expected to have a zero deformation and deflection at the wing's root chord since fixed support is applied. As there are many ribs in the wing structure, bending in the chord-wise direction can be produced when a pressure load is applied. Thus, bending in a chord-wise direction is expected to be present as several ribs are installed in the wing structure. After that, for the fourth mode of vibrations, a pure twisting mode of failure occurs when the natural frequency is 8.0048 Hz. As shown in Fig. 12b, c, the wing experienced a twisting failure in the counter-clockwise direction. But, the maximum value of deformation is coming from the secondary spar near the trailing edge. It shows a swollen spar between the fourth and fifth ribs from the wing structure's root chord. The maximum value of 0.046513 m is produced due to the secondary spar's inefficiency to resist and withstand the pressure load applied to the wing. The zero deformation happened at the wing structure's root chord; since fixed support is implemented, there is to be a connection between the wing and fuselage. Comparatively, the twisting

deformation developed at the leading edge and trailing edge is about 0.020672 m (Fig. 12d).

Besides, the straight wing with primary and secondary square spars developed numbers of deflection between the fourth and seventh ribs for the fifth mode of vibrations. The maximum total deformation is about 0.19831 m located between the fifth and sixth ribs, as shown in Fig. 12e. This modal shape is generated when the frequency is 11.372 Hz. In general, the wing skin structure is not experienced any significant deformation except for the primary and secondary spars. But, in the aerospace studies and aviation industries, any small failure and deformation will significantly fatalities. Therefore, any distortion and failures should be avoided at all costs. Finally, the sixth mode of vibrations occurs when the natural frequency is 11.612 Hz. When the straight wing with square spars and ribs underwent a natural frequency of 11.612 Hz, a significant deflection of the secondary spar is observed with a 0.12393 m bend in the vertical direction. As seen from Fig. 12f, the maximum deformation happens between ribs number four and five from the wing structure's root chord. No distortion is developed at the root chord of the wing. Again, this is due to the fixed support available at one end of the wing, which is at the root. Additionally, the significant deformation of the wing is caused by the insufficient strength of the secondary spar. The secondary spar's inefficient factor leads to a swollen defect on the top of the wing structure. Therefore, it can be concluded that the square cross-section spar is not the right choice of selection to be used as the primary and secondary spars in the wing structure.

#### 4.2.2 Design 2: straight wing with I beam spars

The first mode of vibration for the second design of the wing model, a straight wing configured with I-shaped cross-section spars and ribs, is a pure bending mode in a vertical direction with a natural frequency of 2.3477 Hz. The wing structure appears to have bend upward in a vertical direction. This is because the wing is tending to bend about the root section's minimum moment of inertia. Besides, there is no support at the top chords of the wing to resist and overcome the applied load in the *y*-direction, which is located at the bottom of the wing. It is seen in Fig. 13a that the maximum total deformation is developed at the tip chords of the wing with 0.01283 m while there is no deformation happened at the root. It can be seen that the maximum strain is developed at the trailing edge of the tip chord. The second mode of vibrations for straight wing configured with two I-shaped cross-section spars and ribs, a pure bending mode in the chord-wise direction, is built when a natural frequency is 5.8533 Hz. The wing model experienced a bending failure in the horizontal direction, and the wing is bent towards the trailing edge. It is observed from the front view of Fig. 13b that the maximum deflection happens at the trailing edge of the wing with 0.013819 m of deformation, whereas there is no deformation occurring at the root chord of the wing. As mentioned earlier in two or three analyses before, it is expected to have a zero deformation and deflection at the wing's root chord since fixed support is applied. Additionally, since there are many ribs in the wing structure, bending in the chord-wise direction can be produced when a pressure load is applied. Thus, bending in a chord-wise direction is expected as many ribs are installed in the wing structure.

The third modal shape of straight-wing configured with I-shaped cross-section spars and ribs, the deformation developed, is a pure bending mode in the vertical direction when the wing structure is excited with a natural frequency of 8.8976 Hz. As shown in Fig. 13a, b, the wing experiences a bending failure in the vertical direction, with two areas having a significantly larger deflection. One of the regions is at the wingtip, as the wing experienced 0.012498 m of total deformation. Another one is located between the fifth and sixth ribs from the wing structure's root chord with the same amount of strain. It can be stated that the primary and secondary spars significantly cause deflection since the spars will take most of the load during flight and the weight of the wing while on the ground. The wing skin also will make the bending moment of the wing. Besides, a different thing happened at the wing's root chord, where there is no deformation. This is due to the reaction forces produced when fixed support is applied to connect the wing and fuselage (Fig. 13c).

When the straight wing is configured with the I-shaped cross-section spars and ribs, the fourth mode of vibration is excited with a natural frequency of 19.938 Hz, a pure bending mode in the vertical direction developed along the span of the wing structure. Figure 13d shows that two areas have failed and deformed significantly between the fourth and fifth ribs and between the seventh and eighth ribs from the root chord of the wing. The direction of the bending for both areas is different from each other. One deformation is a bending mode in a positive *y*-axis direction while the other one is in a negative *y*-axis direction. Regardless of their differences in deflection, both areas developed the same amount of deformation, which is 0.0179 m. Besides, it is observed from Fig. 13d that the highest strain is due to the deflection of the internal components of the wing, which is the secondary spar. This is true that the spars will take most of the load when the aircraft is flying and its weight when the aircraft is on the ground. On the other hand, at the root chord of the wing structure, there is no deformation when a pressure load is applied.

In the fifth mode of vibrations, a pure twisting mode of failure occurs when the natural frequency is 24.704 Hz. As shown in two Fig. 13c, d, the wing experienced a twisting failure in the clockwise direction. But, the maximum value of deformation is coming from the secondary spar near the trailing edge. It shows that a swollen wavy spar started from

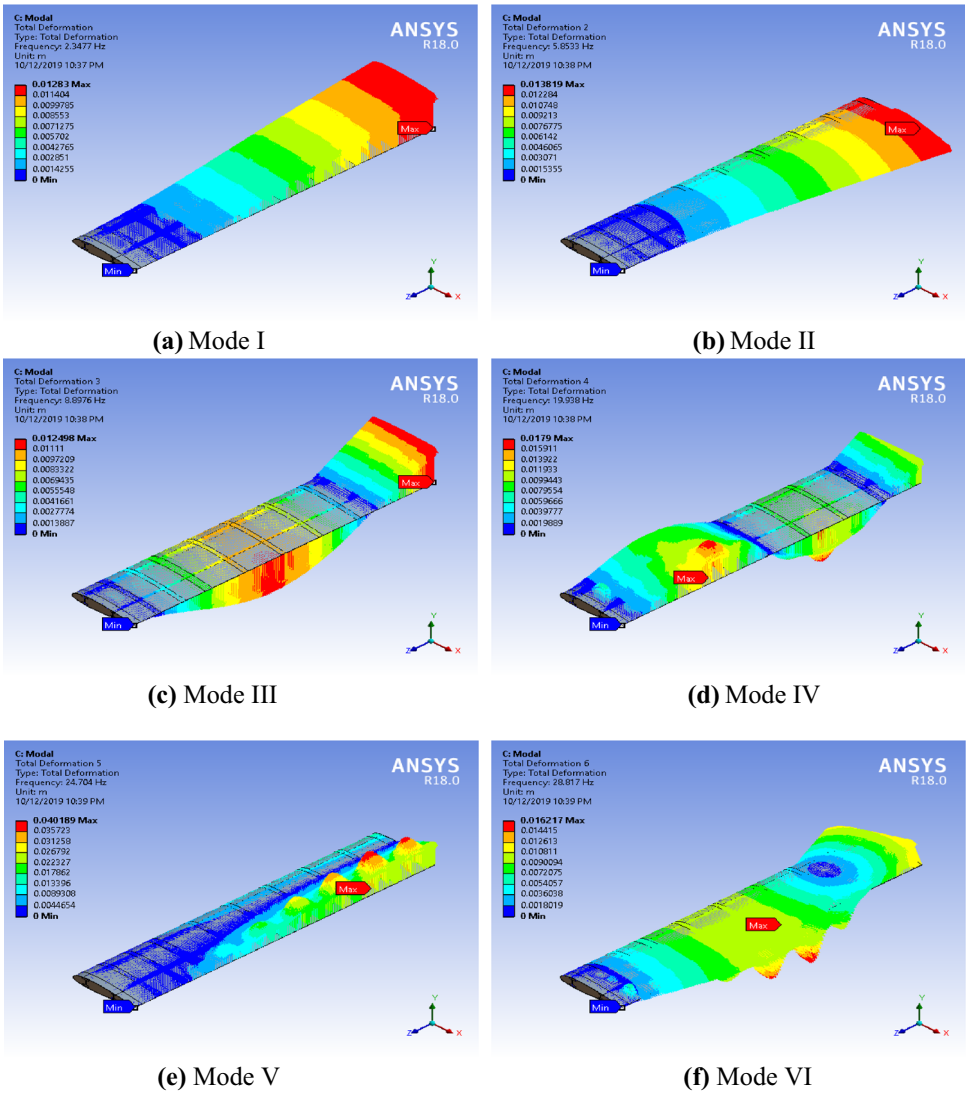


**Fig. 13** Model analysis of straight-wing configured with I-shaped cross-section spars

the fourth ribs to the wing's tip chord. This is due to the buckling of the secondary spars, which then affected the wing structure. The maximum value of 0.040189 m is produced due to the secondary spar's inefficiency to resist and withstand the pressure load applied to the wing. Somehow, at the leading edge of the wing structure, there is no sign of failure caused by the original spars. This shows that the original spars can withstand the applied pressure load at the bottom of the wing. Comparatively, the twisting deformation developed at the leading edge and trailing edge is about 0.022327 m (Fig. 13e).

The last and the sixth modes of vibrations for straight wing configured with two I-shaped cross-section spars and ribs, a combination of bending and twisting mode, are built up when a natural frequency is 28.817 Hz. The wing model experienced a bending failure in the horizontal direction and a twist in a clockwise direction. It is observed from the isometric view of Fig. 13f that a twist is happening between number eighth and ninth ribs from the root chord. In addition to the twisting mode, the wing structure's tip chord is experiencing a bending mode, and hence a combination of twisting and bending mode is observed at the tip chord. Furthermore, the maximum total deflection is built up between the sixth rib and seventh rib from the wing's root chord, whereas zero deformation happening at the root chord of the wing. The maximum value of deformation at the location stated below is 0.016217 m. Additionally, since there are many ribs in the wing structure, bending in the chord-wise direction can be produced when a pressure load is applied. Thus, bending in a chord-wise direction is expected to be present as some ribs are installed in the wing structure.

#### 4.2.3 Design 3: tapered wing

Figure 14a shows the maximum total deformation and deflection of tapered wing configured without any internal ribs and

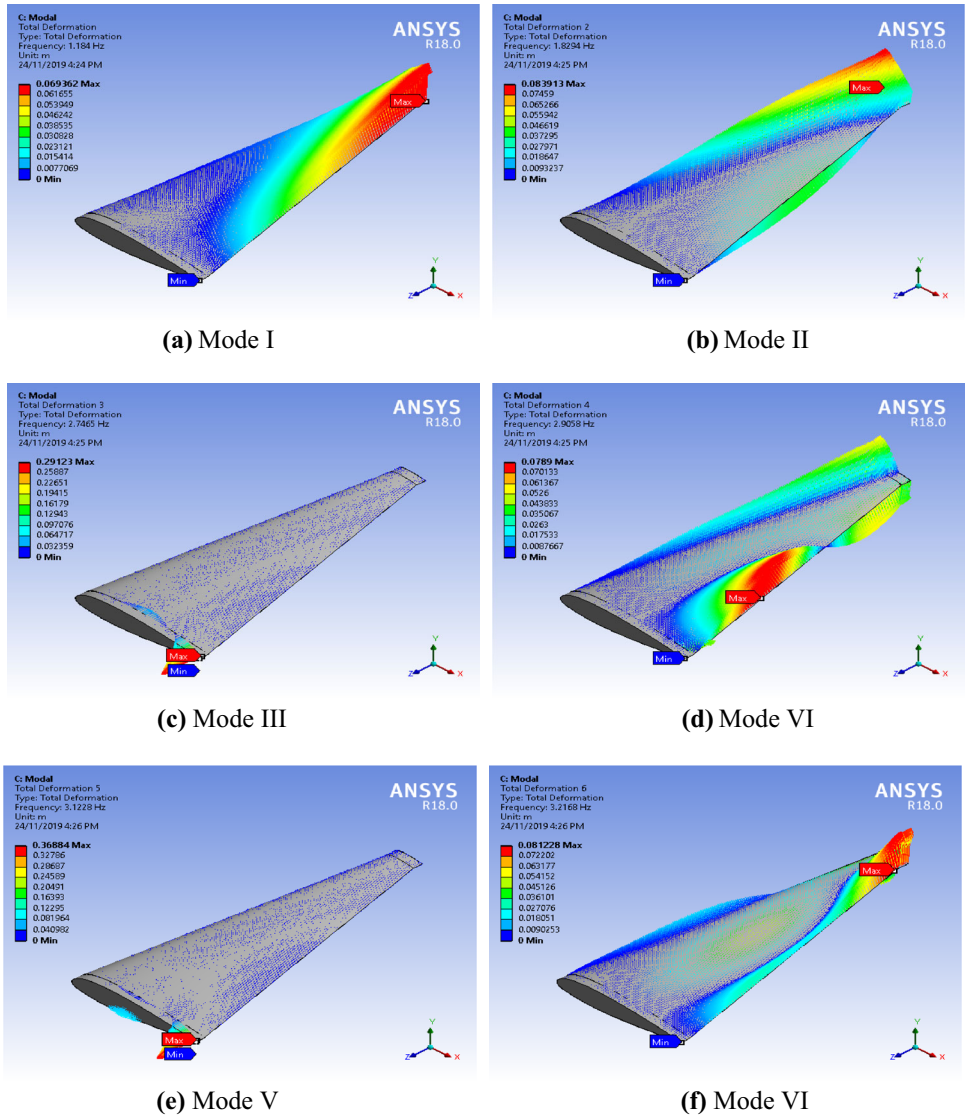


**Fig. 14** Model analysis of tapered wing configured without internal ribs and spars

**Table 5** Modal analysis of straight wing with solid square spars and ribs

| Order | Frequency, $f$ (Hz) | Modal shape | Axis of deflection | Largest deformation, $\Delta L(m)$ |
|---|---|---|---|---|
| 1 | 0.64301 | Bending | $y$-axis | 0.012837 |
| 2 | 4.1950 | Bending | $y$-axis | 0.019954 |
| 3 | 4.6392 | Bending | $x$- and $y$-axes | 0.013219 |
| 4 | 8.0048 | Twisting | – | 0.046513 |
| 5 | 11.372 | Bending | – | 0.198311 |
| 6 | 11.612 | Bending | – | 0.12393 |

spars structure developed at the trailing edge of the wingtip of the wing. Besides, the total deformation built upon this wing structure is a combination of bending and twisting modes. In particular, the total deformation is building up at the trailing edge of the wingtip. This is a precise observation that bending, and a twisting mode of deformation are developed at that location. This resulted in a 0.069362 m of deflection at the trailing edge of the wingtip alone since the highest total deformation is located. No deformation and deflection happened at the root of the wing since fixed support is applied there as in the assembly of an aircraft, the root of wing structure is being fixed at the body fuselage. The total deformation can be developed if and only if the wing structure is excited with a natural frequency of 1.184 Hz.

Figure 14b shows the maximum deformation and deflection of a tapered wing configured without any internal ribs

**Table 6** Modal analysis of straight-wing with I-shaped spars and ribs

| Order | Frequency, $f$ (Hz) | Modal shape | Axis of deflection | Largest deformation, $\Delta L(m)$ |
|---|---|---|---|---|
| 1 | 2.3477 | Bending | $y$-axis | 0.01283 |
| 2 | 5.8533 | Bending | $x$- and $y$-axes | 0.013819 |
| 3 | 8.8976 | Bending | – | 0.012498 |
| 4 | 19.938 | Bending | – | 0.0179 |
| 5 | 24.704 | Twisting | – | 0.040189 |
| 6 | 28.817 | Twisting + bending | – | 0.016217 |

**Table 7** Modal analysis of tapered wing without internal spars and ribs

| Order | Frequency, $f$ (Hz) | Modal shape | Axis of deflection | Largest deformation, $\Delta L$(m) |
|---|---|---|---|---|
| 1 | 1.184 | Bending | $y$-axis | 0.069362 |
| 2 | 1.8294 | Bending | $y$-axis | 0.083913 |
| 3 | 2.77465 | – | – | 0.29123 |
| 4 | 2.9058 | Twisting | – | 0.0789 |
| 5 | 3.1228 | – | – | 0.36884 |
| 6 | 3.2168 | Twisting | – | 0.081228 |

and spar's structure developed at the leading edge of the wingtip. This is different from the first mode of vibrations since, on the first modal shape, the highest total deformation built up at the trailing edge of the tip chord. It is seen that the total strain that has built up on this wing structure is a combination of bending and twisting modes. The overall deformation is building up at the leading edge of the wingtip. This is a precise observation that bending as well twisting mode of deformation is developed at that location. This resulted in 0.083913 m of deflection at the leading edge of the wingtip alone since it is where the highest total deformation is located. No deformation and deflection happened at the root of the wing since fixed support is applied in the assembly of an aircraft. The root of the wing structure is being set at the body fuselage. Therefore, there is no deformation developed at the root of the wing. With this in mind, this total deformation can only be created if and only if the wing structure is excited with a natural frequency of 1.8294 Hz.

The third mode of vibration for the tapered wing configured without any internal ribs and spars experienced a very minimal deformation, except for about 0.29123 m of total strain at the trailing edge of the root chord of the wing structure (Fig. 14c). When the tapered wing is configured without any internal components such as ribs and spars, the fourth mode of vibration is excited with a natural frequency of 2.9058 Hz, a pure twisting mode in the counter-clockwise direction is developed along the chord-wise of the wing structure. As seen from Fig. 14d, there is only one area that has failed and deformed significantly, which is approximately at the trailing edge of the quarter of the total span of the wing structure measured from the root chord wing. This may be due to the taper effects affecting the wing structure to resist the applied pressure load differently compared to the constant chord wing.

The total deformation at about a quarter of the entire span of the wing is 0.0789 m. There is no deformation at the root chord of the wing structure when a pressure load is applied. The fifth mode of vibration for the tapered wing configured without any internal ribs and spars experienced a very minimal deformation in general, except for about 0.36884 m of total strain at the trailing edge of the root chord of the wing structure (Fig. 14e). The sixth mode of vibrations for the tapered wing configured with no internal components such as ribs and spars is shown in the three Fig. 14c–e. The sixth mode of vibration for this wing model shows a pure twisting mode in the clockwise direction. This kind of deformation can only be developed when the wing structure is excited with a natural frequency of 3.2168 Hz. It found that the twisting mode started from the trailing edge and then went down to the leading edge of the tip chord. In Fig. 14f also, it is seen that the wing trailing edges are deformed to the extent of the trailing edge is located upward than the leading edge. Hence, this shows that the wing structure's twisting is developed during this kind of natural frequency. The maximum value of the total deformation is about 0.081228 m. There is no deformation happening at the root chord of the wing.

### 4.3 Discussion and comparison on model analysis

After doing the model analysis of all three designs of 3D wings with six different deformations, it has been found that each method has its advantages in structural analysis and modes. Indeed, the secondary part of the wing is more effective in absorbing the external loads and controlling structural stability. However, the tapered wing is more promising in

aerodynamic conditions and will be advantageous to reduce the drag effects and beneficial to fluid–structure interaction effects. Spars and ribs of the wing also influence the structural control, and this will result in any moment such as bending and twisting will be easy to control and can carry a maximum load that we can see in Fig. 12. Design 2 with I-shaped spars and ribs has minor variations in results, but in this case, the total load of the wing was less as compared to the square shape of ribs and spars. It has been concluded that based on the present model analysis of three different types of wings, each wing has the advantage. Nevertheless, the maximum carrying external pressure with less weight of the wing was found in design 2. In contrast, design 1 has maximum deformation and model frequency, but as a result, the shape of secondary structures has a square which will result in a small increment in the wing total weight. However, design 3-focused more on the shape of the wing with a solid part of the secondary structures. It has more advantages on carrying aerodynamics loads due to tapered ratio and fluid–structure interaction. Moreover, the tapered design also found good results in model analysis.

The modal analysis's goal is to determine the resonance frequencies of the wing structure computationally as structure oscillations at resonance frequencies are often dangerous because relatively small excitation forces result then in large-amplitude vibrations, which can lead to failure of the structure. Thus, to prevent such a resonance phenomenon, it is necessary to investigate under what conditions the resonance occurs. Tables 5, 6, 7 show the overview of all results.

## 5 Conclusions

Three-dimensional wings' structural behaviour has been observed with an independent analysis of the wing structure's three separate design options, and conclusions have been made based on the results and discussions. The verification of past studies' findings using ANSYS simulations is assumed to be accurate and credible as the percentage error is allowable. The static structural analysis shows that the wing structure with I-shaped spars has a better efficiency in resisting bending moment than the other wing structure. This is due to the spars' contribution that supports large loads tending to bend and twist the wing. The deformation of the wing structure and the resonance frequencies have also been detected by modal analysis and found that comparatively, small excitation forces result in large-amplitude vibrations, leading to structural failure. Finally, the current investigation proved that the finite element analysis would help optimize the structural analysis of any large or small object with proper modelling, meshing, and boundary conditions.

**Acknowledgements** This research is supported by the Structures and Materials (S&M) Research Lab of Prince Sultan University.

**Author contributions** A.A. was the adviser of the work and contributed to the FEA simulations, analysis of data and writing the original manuscript. M.A.M.B.M.Z. simulated the numerical results and drafted the manuscript. S.A.K. was the main supervisor of the work and contributed to the analysis of data and reviewing the manuscript. Y.E.I. was contributed to the manuscript by reviewing and editing its contents.

**Data availability** The data that support the findings of this study are available from the corresponding author upon reasonable request.

## Declarations

**Conflict of interest** We wish to confirm that there are no known conflicts of interest associated with this publication and there has been no significant financial support for this work that could have influenced its outcome.

## References

1. Abbas Y, Elsonni T, Abdulmajid AA, Khalafallh A, Alnazir M (2021) Structural analysis of a transport aircraft wing. INCAS Bull. 13(1):3–9. https://doi.org/10.13111/2066-8201.2021.13.1.1
2. ANSYS Inc (2017) ANSYS FLUENT 18.0: theory guidance. Canonsburg, PA
3. Arun Kumar KN, Lohith N, Ganesha BB (2012) Effect of ribs and stringer spacings on the weight of aircraft structure for aluminum material. J Appl Sci 12(10):1006–1012
4. Candade AA, Ranneberg M, Schmehl R (2020) Structural analysis and optimization of a tethered swept wing for airborne wind energy generation. Wind Energy 23(4):1006–1025. https://doi.org/10.1002/we.2469
5. Epstein B, Jameson A, Peigin S, Roman D, Harrison N, Vassberg J (2012) Comparative study of three-dimensional wing drag minimization by different optimization techniques. J Aircr 46(2):526–541. https://doi.org/10.2514/1.38216
6. Flax AH (1943) Three-dimensional wing flutter analysis. J Aeronaut Sci 10(2):41–47
7. Garmann DJ, Visbal MR, Orkwis PD (2014) Three-dimensional flow structure and aerodynamic loading on a revolving wing. Phys Fluids 034101(2013):27. https://doi.org/10.1063/1.4794753
8. Garre P (2017) Modeling and analysis of a RIBS and spars of an airplane wing for bending and shear loads. Int J Res Appl Sci Eng Technol 5(2):295–315. https://doi.org/10.22214/ijraset.2017.2046
9. Jongerius SR, Lentink D (2010) Structural analysis of a dragonfly wing. Exp Mech 50(October):1323–1334. https://doi.org/10.1007/s11340-010-9411-x
10. Khan SA, Aabid A (2018) Design and fabrication of unmanned arial vehicle for multi-mission tasks. Int J Mech Prod Eng Res Dev IJMPERD 8(July):475–484
11. Konayapalli SR, Sujatha Y (2015) Design and analysis of aircraft wing. Int J Mag Eng Technol Manag Res 2(9):167
12. Kumar AR, Balakrishnan SR, Balaji S (2013) Design of an aircraft wing structure for static analysis and fatigue life prediction. Int J Eng Res Technol 2(5):1154–1158
13. Lorber PF (1992) Compressibility effects on the dynamics stall of a three-dimensional wing. In: 30th aerospace science meeting and exhibit, vol 18

14. Lu Y, Shen GX (2008) Three-dimensional flow structures and evolution of the leading-edge vortices on a flapping wing. J Exp Biol 211:1221–1230. https://doi.org/10.1242/jeb.010652
15. Obert E (2009) Aerodynamic design of transport aircraft. IOS Press, Delft University Press, Amsterdam
16. Ohmichi Y, Ishida T, Hashimoto A (2017) Numerical investigation of transonic buffet on a three-dimensional wing using incremental mode decomposition. AIAA SciTech Forum. https://doi.org/10.2514/6.2017-1436
17. Raymer DP (1992) Aircraft Design: A Conceptual Approach (Second Edi). American Institute of Aeronautics and Astronautics Inc, Washington, DC
18. Vani PS, Reddy DVR, Prasad BS, Shekar KC (2014) Design and analysis of A320 wing using E-glass epoxy composite. Int J Eng Res Technol 3(11):536–539
19. Vaquer-araujo X, Schöttle F, Kommer A (2018) Static and dynamic load superposition in spacecraft structural analysis. Adv Aircr Spacecr Sci 5(2):259–275
20. Wang L, Tian FB (2020) Numerical study of sound generation by three-dimensional flexible flapping wings during hovering flight. J Fluids Struct 99:103165. https://doi.org/10.1016/j.jfluidstructs.2020.103165
21. Yang ZR, Jiang Y, Huang C (2015) The thickness of an aircraft wing skins optimization based on ABAQUS. Appl Mech Mater 716–717:679–681
22. Zakuan MAMBM, Aabid A, Khan SA (2019) Modeling and structural analysis of three-dimensional wing. Int J Eng Adv Technol 9(1):6820–6828. https://doi.org/10.35940/ijeat.A2983.109119
23. Zhang X, Zhao Y, Si F (2018) Analysis of wing flexure deformation based on ANSYS. In: 2018 IEEE/ION position, location and navigation symposium, PLANS 2018—Proceedings, pp 190–196. https://doi.org/10.1109/PLANS.2018.8373381